Nanoscale

PAPER

View Article Online
View Journal | View Issue





Cite this: *Nanoscale*, 2018, **10**, 8496

# Electrical modulation of a photonic crystal band-edge laser with a graphene monolayer†

Hanbit Kim,[a,b] Myungjae Lee,[a,b] Hyunhak Jeong,[a] Min-Soo Hwang,[c] Ha-Reem Kim,[c] Seondo Park,[a] Yun Daniel Park,[a,d] Takhee Lee,[a,d] Hong-Gyu Park[c,e] and Heonsu Jeon*[a,b,d]

Received 26th February 2018,
Accepted 2nd April 2018

DOI: 10.1039/c8nr01614c

rsc.li/nanoscale

The electrical control of photonic crystal (PhC) lasers has been an attractive but challenging issue. Laser operation by electrical injection is of key importance for the viability and applicability of the PhC lasers. Another key factor is the electrical modulation of the laser output. The Fermi level of a graphene monolayer can be controlled by electrical gating, which adjusts its optical absorption. In this study, a graphene monolayer sheet is integrated on top of a two-dimensional PhC structure composed of InGaAsP multiple-quantum-wells (MQWs) in order to demonstrate the electrical modulation of a high-power (microwatt-scale) PhC band-edge laser. The introduced dielectric spacer layer presets the delicate balance between the optical gain from the MQWs and optical loss at the graphene monolayer. The proposed device is covered by an ion-gel film, which enables a low-voltage laser modulation at $|V_g| \leq 1$ V. The modulation is extensively investigated experimentally, and the obtained results are confirmed by performing numerical simulations.

## Introduction

Since its discovery, graphene, a two-dimensional (2D) carbon atom network arranged in a honeycomb-lattice, has been attracting enormous attention owing to its unique physical properties, such as strong mechanical tensile strength,[1] high charge-carrier mobility,[2,3] large thermal conductivity,[4] *etc*. In terms of optical properties, graphene is a broadband optical absorber; a single graphene monolayer sheet can absorb as much as ~2.3% of the incident light despite its extremely short atomic-scale optical path length.[5] Using these outstanding properties, many graphene-based photonic devices have been developed, including broadband polarizers,[6] optical modulators,[7] and ultrafast photodetectors.[8]

It is worth noting that the optical absorption by graphene can be directly controlled by tuning the Fermi-level, which can be accomplished by electrical gating[9] or chemical doping.[10] Between the two methods, electrical gating is preferred owing to its compatibility with optoelectronic devices, which provides higher application potential. In principle, absorption by graphene can be modulated at high speed and low power consumption owing to the high carrier mobility of graphene. However, the specific capacitances that can be obtained using conventional gate dielectrics, such as $SiO_2$, $Al_2O_3$, and $HfO_2$, are in the range of 10–1000 nF cm$^{-2}$,[11–13] which is too small to affect the Fermi level of graphene at low gate voltages. This challenge can be overcome by utilizing electrolyte gating, where an ion-gel film is employed as the gate dielectric. An ion-gel consists of an ionic liquid that has a high ion conductivity and a triblock copolymer that forms a cross-linked network. It exhibits a very large specific capacitance ($C \approx 10$ μF cm$^{-2}$),[13–15] which provides Fermi-level tuning at low gate voltages of a few volts, owing to the nanometer-thick electrical double layers (EDLs) formed at the interface between the electrolyte and electrode.[12,16] Furthermore, an ion-gel can be prepared at low temperatures and transferred in a solvent-free environment; hence, it can be applied to almost any substrates.[13]

Graphene has been employed in photonic crystal (PhC) structures to induce extraordinary photonic properties, as reported in the pioneering studies on the enhanced optical absorption by a graphene-capped passive PhC nano-cavity.[17–19] Recently, the group of one of the coauthors of this study employed the above idea in a PhC cavity laser, an active photonic device that has a wavelength-sized tiny cavity, in order to electrically modulate the laser output.[20] Although a cavity-

[a]*Department of Physics and Astronomy, Seoul National University, Seoul 08826, Republic of Korea. E-mail: hsjeon@snu.ac.kr*
[b]*Inter-University Semiconductor Research Center, Seoul National University, Seoul 08826, Republic of Korea*
[c]*Department of Physics, Korea University, Seoul 02841, Republic of Korea*
[d]*Institute of Applied Physics, Seoul National University, Seoul 08826, Republic of Korea*
[e]*KU-KIST Graduate School of Converging Science and Technology, Korea University, Seoul 02841, Republic of Korea*

†Electronic supplementary information (ESI) available. See DOI: 10.1039/c8nr01614c

based PhC laser consumes very low power, which makes it applicable as a single photon source, it may not be suitable for future photonic integrated circuits (PICs), owing to its low laser output power and fixed laser emission direction (only along the direction perpendicular to the 2D PhC plane, unless the quality factor $Q$ of the cavity is intentionally deteriorated). In this context, photonic band-edge (PBE) lasers could be more desirable for PIC applications. PBE lasers are a special type of PhC laser; they have a fully periodic structure without defects and exhibit a standing-wave modal profile. The output power of a PBE laser can be easily scaled by adjusting the active device area. In addition, the direction of the laser emission can be tailored by controlling the PBE modes; while the PBE mode at the Brillouin zone center (Γ-point) offers a vertical laser emission, the PBE mode at the zone boundary results in an in-plane laser emission.[21] In this study, we demonstrate a direct modulation of the laser output by electrical tuning of the Fermi-level of a graphene monolayer sheet attached to a PBE laser device. The electrical modulation is facilitated at a low gate voltage operation by electrolyte gating, where the graphene sheet is covered by an ion-gel film. We observe that the high output power from an optically excited PBE laser can be enhanced or reduced (partially or completely) by applying a DC gate voltage smaller than 1 V.

## Results and discussion

Fig. 1a shows a schematic of the device structure. A honeycomb-lattice 2D PhC pattern was generated on an InP-based multiple-quantum-well (MQW) epilayer using electron-beam lithography. The PhC pattern was then transferred to the underlying MQW layer using a reactive-ion etch, followed by a selective wet chemical etch of the InP etch-sacrificial layer underneath the MQW epilayer to produce an air-bridge type PhC PBE laser device. A 60 nm-thick $SiO_2$ spacer layer was then deposited on top of the PhC PBE laser using plasma-enhanced chemical vapor deposition. Subsequently, a graphene monolayer sheet was transferred on the obtained structure. The $SiO_2$ spacer layer determines the distance between the MQW slab waveguide and the graphene sheet, which affects the degree of optical loss at the graphene sheet. After the deposition of a Ti/Au electrode on the PhC device and a microscope slide using an electron-gun evaporator, the PhC device was mounted on the microscope slide. Then, an ion-gel film was attached to the entire structure to complete the device fabrication (see the ESI† for a detailed description). Fig. 1b shows a photograph of the fabricated device. The area enclosed by the red square corresponds to the illustration in Fig. 1a. The rounded blue box approximately outlines the boundary of the ion-gel film. Fig. 1c shows a scanning electron microscopy (SEM) image of the 2D PhC pattern. Although it is challenging to notice it in the figure, the PhC structure is actually covered by a graphene layer, which indicates the high-quality growth and transfer of the graphene monolayer sheet. The distance between two nearest air-holes is $a$ = 450 nm, while the air-hole radius is $r = 0.32a$. Fig. 1d shows the corresponding photonic band structure of the honeycomb-lattice PhC membrane structure, calculated for the transverse-electric (TE) polarization using the plane-wave-expansion (PWE)

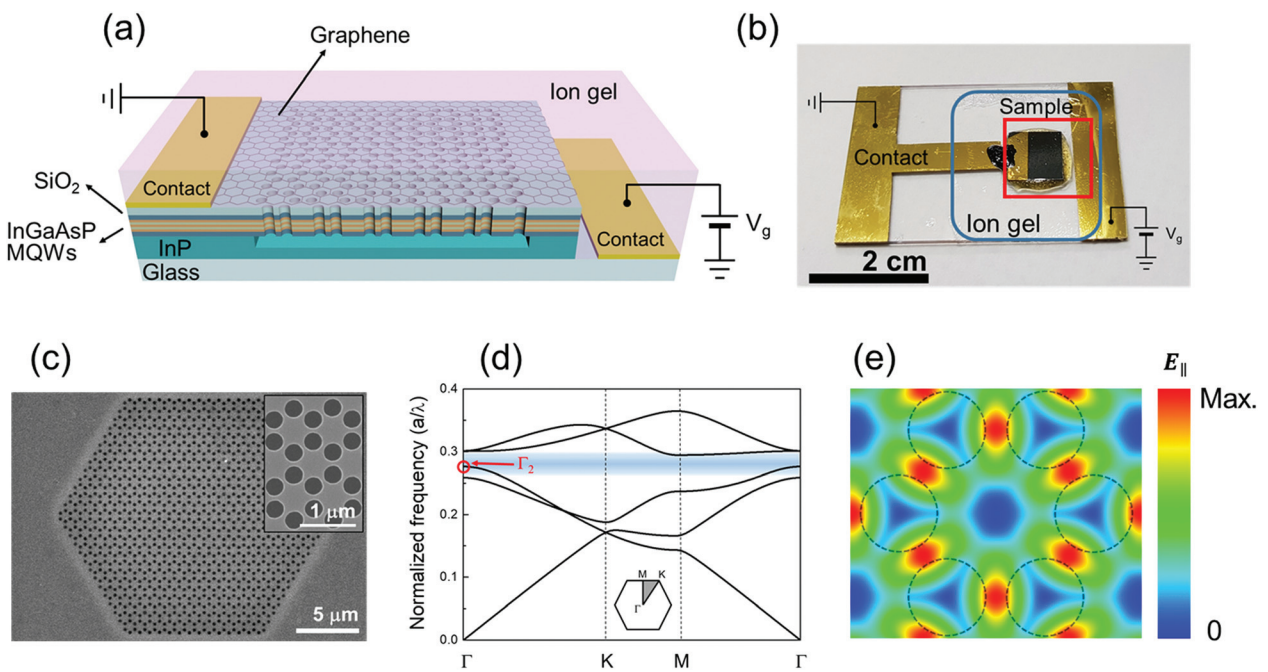


**Fig. 1** PhC-graphene device structure. (a) Schematic of the entire device structure. (b) Photograph of the fabricated device. (c) SEM image of the graphene-covered PhC structure. The inset shows a magnified image. (d) Calculated band structure for the PhC structure that has a honeycomb lattice. (e) Transverse electric field profile.

method. For modeling, all structural parameters were chosen such that the second zone center PBE mode ($\Gamma_2$) matches with the emission band of the InGaAsP MQW, which is shaded in light-blue in the figure. Fig. 1e shows the transverse-electric field ($E_{\parallel} = \sqrt{E_x^2 + E_y^2}$) distribution profile of the $\Gamma_2$ PBE mode, calculated using the finite-difference time-domain (FDTD) method. One can easily notice that the high-electric-field region significantly overlaps with the active MQW region.

The Fermi level of a monolayer graphene can be tuned across the Dirac point by electrical gating.[22] In order to ensure that our graphene sheet is a high-quality monolayer, we performed Raman spectroscopy measurements. For this purpose, we prepared a dedicated sample by directly transferring a graphene sheet onto a 100 nm-thick $SiO_2$ layer deposited on a silicon substrate. Fig. 2a shows a Raman spectrum of the graphene sample. We can clearly identify both G and 2D peaks. In particular, the 2D peak at ~2700 $cm^{-1}$ is a direct proof of the existence of a graphene monolayer sheet.[23] The intensity ratio between the two peaks is $I_{2D}/I_G \approx 1.5$, which is much lower than the values observed by others, indicating that our graphene layer is not neutral but doped unintentionally.[24] In addition, the D peak (at ~1350 $cm^{-1}$) is negligible, which suggests that our graphene sheet has a high quality and a very low amount of defects created during the growth and transfer process.[25]

In order to demonstrate the effects of electrical gating on the optical absorption by graphene, we prepared a blank device, composed of a graphene monolayer, electrode, and ion-gel film, produced on a microscope slide. The blank device is almost the same as the full device shown in Fig. 1a, except for the lack of the PBE laser and $SiO_2$ spacer layer. We then applied a gate voltage to the blank device and investigated the changes of the optical transmittance through the graphene sheet, using a 1550 nm continuous-wave laser diode (LD). The measured transmittance T values in the gate voltage range of $-1.0\ V \le V_g \le 1.0\ V$ are summarized in Fig. 2b. The optical transmittance changes monotonically from ~88.1% at $V_g$ = −1.0 V to ~86.8% at $V_g$ = +1.0 V. The overall trend is in good agreement with the FDTD-calculated transmittance change $\Delta T$ (red curve in Fig. 2b). This demonstrates that with the aid of an ion-gel, the optical loss at the graphene sheet can be controlled by adjusting the gate voltage (smaller than 1 V). For undoped neutral graphene, the Fermi-level tuning occurs either by electron extraction from the valence band or by electron injection into the conduction band, depending on the polarity of the gate bias voltage. The Fermi-level tuning changes the graphene absorption through Pauli blocking. However, for our sample, the charge neutrality, at which the Fermi level is aligned with the Dirac point and the transmittance (absorbance) reaches its minimum (maximum) value, occurred at a positive gate voltage. We believe that this is caused by the unintentional doping of the graphene sheet such that the Fermi level at $V_g$ = 0 V is below the Dirac point. By fitting the measured data with the simulation results, we estimated that the charge neutrality in the graphene sheet was obtained at $V_g \approx 1.25$ V. Therefore, in this study, we adjusted the gate voltage within the negative range of $-1.0\ V \le V_g \le 0$ V. The insets of Fig. 2b illustrate the optical absorption in the unintentionally p-doped graphene.

In order to induce a PBE lasing, the fabricated devices were optically excited using a 1064 nm pulsed LD (500 kHz frequency; 1% duty cycle). For a simultaneous optical excitation and spectral measurement, we employed a compact micro-photoluminescence (μPL) setup based on a 1 × 2 wavelength-division-multiplexing optical fiber coupler.[26] As the fiber probe tip was in close proximity (<30 μm) to the sample during the measurement, the optically excited area (~70 μm in diameter) was estimated to be slightly larger than the core diameter of the optical fiber (62.5 μm). During the pulsed optical excitation, a gate voltage was applied across the ion-gel film using

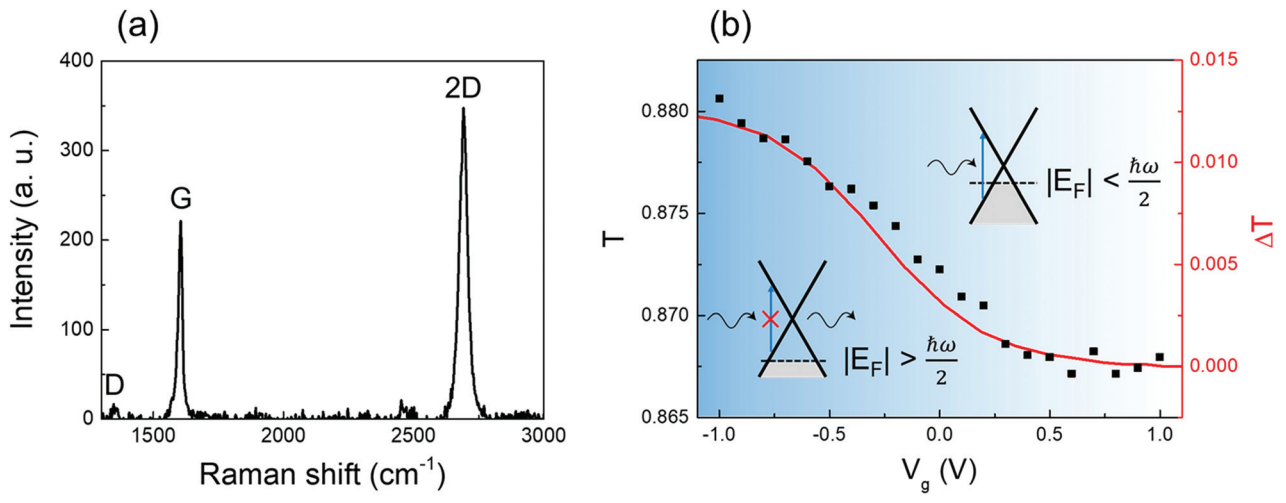


Fig. 2 Monolayer graphene. (a) Raman spectrum of a monolayer graphene sheet. (b) Optical transmittance through a graphene monolayer measured at 1550 nm as a function of the gate voltage. The transmittance is also simulated using the FDTD method. The insets show energy diagrams to illustrate the relationship between the photon absorptions and the Fermi-level position.

 

a DC power supply. We obtained a low leakage current (smaller than 1 μA) for the entire gate voltage range. The μPL spectra were measured at various optical excitation levels and gate voltages to obtain a performance map of the PBE laser (see the ESI†).

Fig. 3a shows the μPL spectra measured at various optical excitation levels; the gate voltage was fixed at $V_g = -1.0$ V. At excitation power densities smaller than ~0.45 kW cm$^{-2}$, we did not observe any sign of lasing. However, at higher excitation densities, a sharp single emission peak emerged, and its intensity continuously increased, which is a clear sign of single-mode lasing with a well-defined threshold. We identified that the lasing peak corresponded to the $\Gamma_2$ PBE mode, as the PhC structure was designed such that the $\Gamma_2$ mode was positioned (spectrally) at the center of the MQW emission band (Fig. 1d). Repeated measurements at different gate

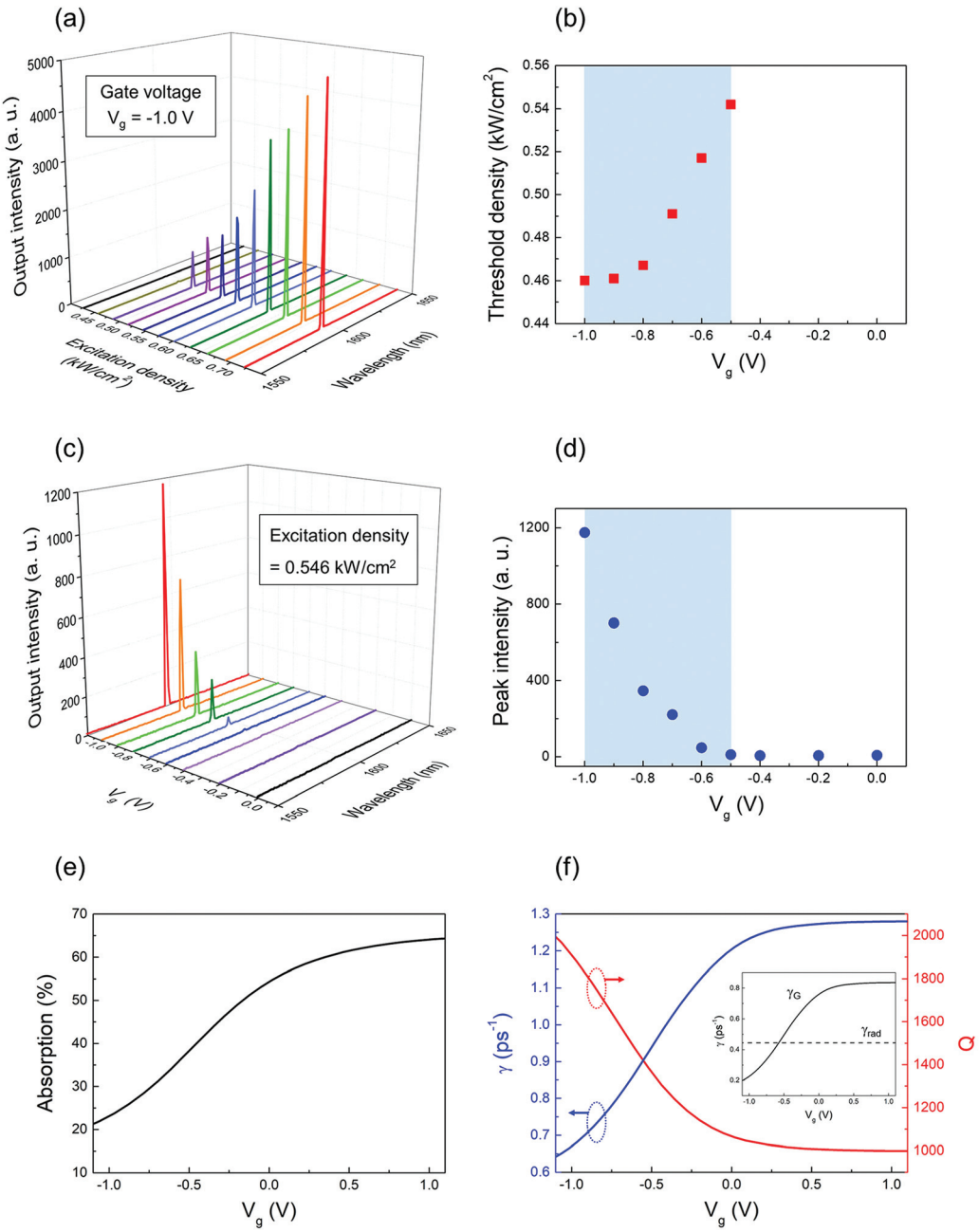


**Fig. 3** Modulation of the band-edge laser. (a) Micro-photoluminescence spectra measured at various optical excitation levels, at a fixed gate voltage of $V_g = -1.0$ V. (b) Laser thresholds determined for different gate voltages. (c) Micro-photoluminescence spectra measured at various gate voltages within the range of $-1.0$ V $\leq V_g \leq 0$ V, at a fixed optical excitation level. (d) Peak laser intensity as a function of the gate voltage, at a fixed optical excitation level. (e) FDTD-simulated optical absorption as a function of the gate voltage. (f) Dependences of the photon decay rate $\gamma$ and cavity $Q$-factor as a function of the gate voltage, obtained by performing FDTD simulations.

voltages showed that the single-mode lasing action was sustained but with different threshold values, as summarized in Fig. 3b. It is shown that the PBE laser threshold rapidly increased with an increase of the gate voltage from ~0.46 kW cm$^{-2}$ at $V_g$ = −1.0 V to ~0.54 kW cm$^{-2}$ at $V_g$ = −0.5 V. These results are a clear indication that the PBE laser performance can be electrically controlled. We did not observe any lasing action for gate voltages larger than −0.5 V, most likely owing to the very high absorption loss at the graphene monolayer.

More relevant for the direct electrical modulation should be the relationship between the laser output and gate voltage. Fig. 3c shows laser spectra recorded for various gate voltages, at a fixed optical excitation power density of ~0.55 kW cm$^{-2}$. For $V_g$ > −0.5 V, there is no (or it is very weak) sign of lasing. However, a well-defined single-mode laser peak appeared at 1596 nm for $V_g \leq -0.5$ V, while the PBE laser output increased monotonously with the decrease of the gate voltage. Fig. 3d summarizes the maximum output intensity as a function of the gate voltage, which directly demonstrates that the PBE laser output can be modulated by applying a gate voltage in the range of $-1.0\ \text{V} \leq V_g \leq -0.5\ \text{V}$.

For a theoretical confirmation, we performed FDTD simulations on a model device structure. Fig. 3e shows the calculated absorption by the graphene monolayer sheet in the PhC-graphene structure. As the interband transitions of electrons are responsible for the optical absorption by the graphene monolayer, the value of the optical power dissipation can be obtained by analyzing the interaction between the corresponding optical conductivity and resonant $\Gamma_2$ PBE mode (a detailed description is provided in the ESI†). Fig. 3e shows that the optical absorption by the graphene monolayer increases with the gate voltage. The general trend is qualitatively consistent with the experimentally determined laser thresholds shown in Fig. 3b. It is interesting to note that the modulation depth in absorption (~40%) is much larger than that in transmittance (~1%) shown in Fig. 2b. This is simply due to the fact that transmittance is measured through the graphene monolayer in the perpendicular direction, whereas absorption is considered for the specific PBE mode employed for lasing action, which oscillates along the sample plane so that its interaction length with graphene is effectively much longer.

In addition, we calculated the photon decay rate in the PhC-graphene structure for various gate voltages, as shown in Fig. 3f. We synchronously excited multiple electric dipoles that were distributed randomly across the device structure and monitored the subsequent time evolution of the accumulated optical power of the $\Gamma_2$ PBE mode. We obtained the value of the photon decay rate $\gamma$ by fitting the results using the equation, $P(t) = P_0 e^{-2\gamma t}$. The simulation results clearly show that the photons decay more rapidly at higher gate voltages; the overall behavior is very similar to the independently calculated optical absorbance data shown in Fig. 3e. As the InGaAsP MQWs are assumed to be lossless in the simulations, the remaining loss mechanisms are the radiation loss (owing to the PhC structure) and optical absorption (by the graphene monolayer). The total decay rate of the PhC-graphene structure can be expressed as: $\tau = \tau_{rad} + \tau_G$, where $\tau_{rad}$ and $\tau_G$ are the decay rates that correspond to the radiation loss and graphene absorption, respectively. However, we can easily distinguish $\tau_G$ from $\tau_{rad}$, as only $\tau_G$ depends on the gate voltage. To clarify this, we performed additional simulations with and without a graphene layer. These results indicate that the background $\tau_{rad}$ is ~0.45 ps$^{-1}$ while the $V_g$-dependent $\tau_G$ varies widely over the range of ~0.2–0.8 ps$^{-1}$ (the inset of Fig. 3f). The $Q$-factor of the cavity can be estimated using the photon decay time ($\tau = 1/\gamma$) and the equation $\tau = 2Q/\omega_0$, where $\omega_0$ is the $\Gamma_2$ resonance frequency. The $Q$-factor obtained is also shown in Fig. 3f.

As mentioned above, the high output power and tailored emission direction are unique advantages of the PBE lasers. Therefore, a successful electrical modulation of a PBE laser could produce a directly modulated large laser power in a pre-

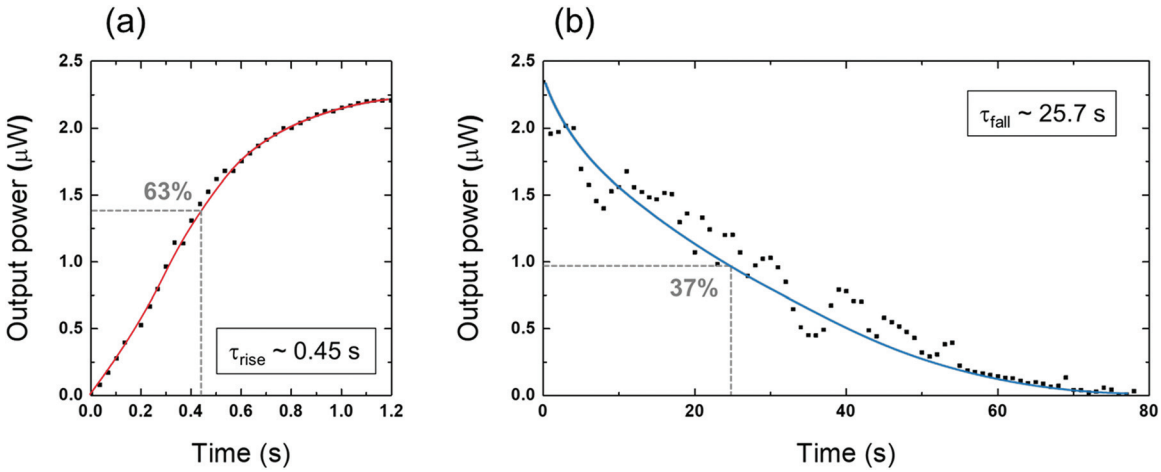


Fig. 4 Temporal response. Measured fiber-coupled laser output power as a function of the time: (a) after the laser turn-on ($V_g$ switched from 0 to −1.0 V) and (b) after the laser turn-off ($V_g$ switched from −1.0 to 0 V).

 

defined emission direction, which is highly desirable for future PIC applications. On the other hand, a fast signal modulation should be of key importance for real applications. In order to assess the modulation characteristics of the proposed device, we examined the temporal response of the PBE laser output to an abrupt change of the gate voltage: from 0 V to −1.0 V for a laser turn-on and from −1.0 V to 0 V for a laser turn-off. The measurements were performed conveniently by connecting the output port of the fiber-based μPL setup to an optical power meter (AQ2201, Yokogawa), instead of a spectrometer. Fig. 4a and b show the time responses to a laser turn-on and turn-off, respectively. Throughout the measurements, the 1064 nm optical excitation power density was fixed at ~0.72 kW $cm^{-2}$. Under this excitation condition, the steady-state PBE laser output power at $V_g$ = −1.0 V was ~2.2 μW. It is worth mentioning that this value of the output power is ~1000 times larger than the nanowatt-level output power of conventional cavity-based PhC lasers.[27] The rise and fall times, estimated by fitting the experimental data in Fig. 4a and b, are $\tau_{rise} \approx 0.45$ s and $\tau_{fall} \approx 25.7$ s, respectively. Both responses are too slow for practical applications. The slow electrical response is an intrinsic issue of the ion-gel, not of the PBE laser or graphene. The ion-gel performance relies on the mobility of the constituent ions inside the electrolyte, which is very low. This notion explains the discrepancy of the rise and fall times. During the turn-on, ions move relatively rapidly in response to the applied electrical field; however, during the turn-off, ions diffuse back to their original random state, which lasts significantly longer. We may expect faster temporal responses of PBE lasers (in principle, of any PhC-based laser) with the introduction of an ion-gel that has a significantly improved ion conductivity or with the use of alternative ingenious electrical methods that can control the Fermi level of graphene.

## Conclusions

In conclusion, we successfully demonstrated a direct electrical modulation of a PBE laser by controlling the Fermi level of the graphene monolayer attached in close proximity to the PBE laser. A low voltage modulation at $|V_g| < 1$ V was achieved by electrolyte gating, where an ion-gel was used as the gate dielectric. By combining a graphene monolayer and an ion-gel film, we showed that a low gate voltage can modify the optical absorption of graphene. Then, we applied the low-voltage electrical gating method to an optically excited InGaAsP MQW PBE laser device. We successfully directly modulated a microwatt-level PBE laser output within gate voltages smaller than 1 V. Although the challenges with the modulation speed remain, this study demonstrates that the graphene monolayer is sufficiently effective to control the performance of various PhC-based photonic devices, which extends the applicability of graphene. We believe that future studies could achieve an electrical modulation of the Fermi level of graphene at low voltages and fast speeds, which can improve the performances of the existing photonic devices.

## Conflicts of interest

There are no conflicts to declare.

## Acknowledgements

This study was supported by the National Research Foundation (NRF) (2014R1A2A1A11051576; 2009-0081565).

## References

1 C. Lee, X. Wei, J. W. Kysar and J. Hone, *Science*, 2008, **321**, 385–388.
2 K. I. Bolotin, K. J. Sikes, Z. Jiang, M. Klima, G. Fudenberg, J. Hone, P. Kim and H. L. Stormer, *Solid State Commun.*, 2008, **146**, 351–355.
3 Y. Zhang, Y. Tan, H. L. Stormer and P. Kim, *Nature*, 2005, **438**, 201–204.
4 A. A. Balandin, S. Ghosh, W. Bao, I. Calizo, D. Teweldebrhan, F. Miao and C. Lau, *Nano Lett.*, 2008, **8**, 902–907.
5 R. R. Nair, P. Blake, A. N. Grigorenko, K. S. Novoselov, T. J. Booth, T. Stauber, N. M. R. Peres and A. K. Geim, *Science*, 2008, **320**, 1308.
6 Q. Bao, H. Zhang, B. Wang, Z. Ni, C. Lim, Y. Wang, D. Tang and K. Loh, *Nat. Photonics*, 2011, **5**, 411–415.
7 M. Liu, X. Yin, E. Ulin-Avila, B. Geng, T. Zentgraf, L. Ju, F. Wang and X. Zhang, *Nature*, 2011, **474**, 64–67.
8 F. Xia, T. Mueller, Y. Lin, A. Valdes-Garcia and P. Avouris, *Nat. Nanotechnol.*, 2009, **4**, 839–843.
9 K. S. Novoselov, A. K. Geim, S. V. Morozov, D. Jiang, Y. Zhang, S. V. Dubonos, I. V. Grigorieva and A. A. Firsov, *Science*, 2004, **306**, 666–669.
10 H. Liu, Y. Liu and D. Zhu, *J. Mater. Chem.*, 2011, **21**, 3335–3345.
11 A. Facchetti, M. Yoon and T. J. Marks, *Adv. Mater.*, 2005, **17**, 1705–1725.
12 J. Cho, J. Lee, Y. Xia, B. Kim, Y. He, M. J. Renn, T. P. Lodge and C. D. Frisbie, *Nat. Mater.*, 2008, **7**, 900–906.
13 K. Lee, M. Kang, S. Zhang, Y. Gu, T. P. Lodge and C. D. Frisbe, *Adv. Mater.*, 2012, **24**, 4457–4462.
14 B. Kim, H. Jang, S. Lee, B. Hong, J. Ahn and J. Cho, *Nano Lett.*, 2010, **10**, 3464–3466.
15 J. Lee, M. J. Panzer, Y. He, T. P. Lodge and C. D. Frisbie, *J. Am. Chem. Soc.*, 2007, **129**, 4532–4533.
16 V. Narasimhan and S. Park, *Langmuir*, 2015, **31**, 8512–8518.
17 X. Gan, K. Mak, Y. Gao, Y. You, F. Hatami, J. Hone, T. Heinz and D. Englund, *Nano Lett.*, 2012, **12**, 5626–5631.
18 A. Majumdar, J. Kim, J. Vuckovic and F. Wang, *Nano Lett.*, 2013, **13**, 515–518.
19 X. Gan, R. Shiue, Y. Gao, K. Mak, X. Yao, L. Li, A. Szep, D. Walker, Jr., J. Hone, T. F. Heinz and D. Englund, *Nano Lett.*, 2013, **13**, 691–696.

20 M. Hwang, H. Kim, K. Kim, K. Jeong, J. Park, J. Choi, J. Kang, J. Lee, W. Park, J. Song, M. Seo and H. Park, *Nano Lett.*, 2017, **17**, 1892–1898.
21 H. Jung, M. Lee, C. Han, Y. Park, K. Cho and H. Jeon, *Opt. Express*, 2017, **25**, 32919–32930.
22 Y. Yu, Y. Zhao, L. E. Brus, K. S. Kim and P. Kim, *Nano Lett.*, 2009, **9**, 3430–3434.
23 A. C. Ferrari, *Solid State Commun.*, 2007, **143**, 47–57.
24 A. Das, S. Pisana, B. Chakraborty, S. Piscanec, S. K. Saha, U. V. Waghmare, K. S. Novoselov, H. R. Krishnamurthy, A. K. Geim, A. C. Ferrari and A. K. Sood, *Nat. Nanotechnol.*, 2008, **3**, 210–215.
25 A. C. Ferrari, J. C. Meyer, V. Scardaci, C. Casiraghi, M. Lazzeri, F. Mauri, S. Piscanec, D. Jiang, K. S. Novoselov, S. Roth and A. K. Geim, *Phys. Rev. Lett.*, 2006, **97**, 187401.
26 C. Han, H. Kim, H. Jung, S. Lee, P. G. Jablonski and H. Jeon, *Optica*, 2017, **4**, 464–467.
27 M. Loncar, T. Yoshie, A. Scherer, P. Gogna and Y. Qiu, *Appl. Phys. Lett.*, 2002, **81**, 2680–2682.